

Vibration-assisted resonance in photosynthetic excitation energy transfer

E. K. Irish* and R. Gómez-Bombarelli

*SUPA and Institute of Photonics and Quantum Sciences,
Heriot-Watt University, Edinburgh, EH14 4AS, United Kingdom*

B. W. Lovett†

*SUPA and Institute of Photonics and Quantum Sciences,
Heriot-Watt University, Edinburgh, EH14 4AS, United Kingdom and
Department of Materials, University of Oxford, Oxford, OX1 3PH, United Kingdom*

(Dated: July 1, 2013)

Coherent quantum energy transfer, as observed in photosynthetic pigment-protein complexes, is inhibited by energetic disorder. While this difficulty can be overcome to some extent by the addition of environmental noise, it has recently begun to be appreciated that discrete intra- and/or intermolecular vibrational modes may play an important role in quantum dynamics. We present a microscopic mechanism by which intramolecular vibrational modes create resonant energy transfer pathways, enhancing the efficiency of both coherent and dephasing-assisted transfer. The principles of this vibration-assisted resonance are illustrated in a simple model based on one energy-transfer branch of the well-characterised Fenna-Matthews-Olson complex. Despite its simplicity, this model captures the interplay between strong electronic coupling that produces delocalised exciton states and resonance-enhanced weak coupling to local vibrational modes. Analytical and numerical results show that intramolecular vibrations can enhance energy transport efficiency and suggest that the vibration-assisted resonance mechanism can overcome some of the limitations of dephasing-assisted transport.

I. INTRODUCTION

In recent years investigations of energy transport in noisy quantum networks have found a surprising and powerful application in the study of light-harvesting systems. The ensuing surge of research has been driven in part by the observation of long-lived quantum coherence in photosynthetic pigment-protein complexes [1, 2] and in part by the prospect of biomimetic improvements to solar energy technology [3]. Of particular interest to theorists is the Fenna-Matthews-Olson (FMO) complex from green sulphur bacteria, both for its small size and consequent mathematical tractability and for the availability of experimental data on its structure, optical properties, and dynamics [1, 2, 4–6]. Hence this unremarkable system has become the primary testing ground for theories of how quantum coherence can survive in noisy, disordered biological conditions.

A major issue for coherent quantum transport in disordered systems, such as those found in FMO and other photosynthetic complexes, is that the detuning of excitation energies between different pigment molecules results in inefficient transport. Even in the case of just two sites, fully coherent Hamiltonian dynamics can only produce full population transfer from one site to the other if the two sites have identical energies. Once the energy difference exceeds the coupling the amplitude of population oscillations is significantly reduced and the excitation be-

comes primarily localised on a single site.

Several studies have shown that dephasing, even in the absence of dissipation, can overcome the localisation effects of quantum coherent dynamics in a disordered system [7–11]. This effect, referred to as dephasing-assisted transport (DAT) or environment-assisted quantum transport (ENAQT), has been explained in several ways. In a static picture, dephasing creates line broadening that increases the overlap between detuned energy levels. The complementary dynamical picture is that the environmentally induced energy fluctuations responsible for dephasing can momentarily bring the energies of two adjacent sites into resonance, allowing efficient transfer between them. Alternatively, the dephasing can be thought of as destroying the phase coherence that causes destructive interference, thereby destroying the localisation. Such noise-assisted models have proved quite successful in explaining how quantum effects may be able to survive under biological conditions.

However, producing highly efficient transport within the appropriate biological timescales using dephasing alone requires some assumptions that can be questioned on physical grounds. In order to achieve one-way energy transport across the molecule rather than simple diffusion, DAT/ENAQT relies on the addition of a trap site to which energy is transferred irreversibly at a constant rate. Although this mechanism is designed to model exciton transfer from the FMO complex to the reaction centre, there is in fact very little experimental data on which to base it [see 12, and references therein]. This issue is discussed in more detail in Sec. III. Another area of concern, which we do not address directly here, is the relative magnitudes of the dephasing rates required to pro-

*Electronic address: e.irish@hw.ac.uk

†Electronic address: b.lovvett@hw.ac.uk

duce efficient energy transfer. When the dephasing rates on each site are optimised independently, the resulting values span two orders of magnitude [7, 9]. In a highly structured pigment-protein complex such as FMO, where the average chromophore separation is on the order of 1.2 nm [6], it seems unlikely that adjacent chromophores experience such drastically different noise levels.

Experiments have revealed rich intramolecular vibrational structures in FMO [13, 14] and other photosynthetic pigment-protein complexes [15, 16]. These vibrational modes correspond strikingly well to exciton energy splittings, offering the tantalising suggestion that resonances between exciton transitions and vibrational modes could play a role in producing effective energy transfer. Numerical results indicate that this may indeed be the case [10, 17–19], although other authors have suggested otherwise [20].

Microscopic mechanisms by which resonant vibrations can contribute to energy transfer are not yet fully understood. Lim *et al.* have developed a model based on coherent interaction of a linear chain of molecules with a shared phonon mode that leads to fast, directional exciton transfer [21]. However, the existence of correlated vibrations across multiple pigments remains controversial [22, 23]. A semiclassical treatment of local vibrational modes was used in Ref. [19] to explain the generation of long-lived coherence via a driven vibration. Kolli *et al.* discussed a dimer interacting with a single quantum mode as a model for the central pigment pair of phycoerythrin 545 in cryptophyte algae [24]. While these studies have shown enhancement of energy transfer in the presence of the vibrational mode(s) considered, none of them have demonstrated that resonance is present or required. Resonance effects on the amplitude and lifetime of coherence oscillations were reported within a dimer model of sites 3 and 4 of FMO [25], but energy transfer was not examined in that study. Resonant enhancement of energy transfer in a model qualitatively similar to that presented here was discussed briefly in Ref. [11] in the context of the phonon antenna mechanism, which postulates that exciton energy splittings matched to peaks in the spectral density create faster transport due to the increased fluctuations [18].

In contrast to previous studies, we consider localised vibrations of the chromophores in a coherent quantum formalism. We construct a simple model that illustrates the mechanism of vibration-assisted resonance whereby a vibrationally excited state creates a resonant pathway for efficient energy transfer. By basing the level structure and parameters on experimental data from FMO, we are able to assess whether the mechanism could plausibly play a role in photosynthetic systems. It must be emphasised, however, that this is a general mechanism that could operate in a variety of systems. An analysis using degenerate perturbation theory provides both an intuitive picture of how vibrational resonance can enable efficient energy transport and an analytical framework for accurately identifying resonance frequencies in a sys-

tem with strong excitonic couplings. Numerical simulations incorporating dephasing and vibrational relaxation demonstrate that vibrational resonance can enhance energy transport, without invoking correlated fluctuations or delocalised phonon modes. Furthermore, our results clearly point out the crucial role of resonance in the enhancement effect. We conclude by assessing the relationship of vibration-assisted resonance to recent experiments and to related theories, and remark on the potential for expanding the model presented here into a fully testable theory.

II. MODEL

To illustrate the vibration-assisted resonance mechanism, we construct a simple model that captures the essential physics, based on sites 1-3 of the FMO complex. To a good approximation, these three sites comprise one of two energy transfer branches identified in FMO [26, 27]. Within Redfield theory, the pigment molecules are described as two-level systems, coupled via an electronic interaction, and interacting linearly with vibrational modes of the pigment-protein complex. Our model, illustrated in Fig. 1, consists of three pigment molecules, or sites, whose electronically excited states are denoted by $|i\rangle$, $i = 1, 2, 3$; the overall ground state of the system is denoted by $|g\rangle$. Sites 1 and 2 are near resonance and strongly coupled, while site 3 has a much smaller excitation energy and is more weakly coupled to the other sites. For simplicity we include only a single vibrational mode of frequency ω , linearly coupled with strength λ to site 3. Furthermore, we restrict the mode to its ground and first excited states; these states are denoted, respectively, by $|3, 0\rangle$ and $|3, 1\rangle$. Within the single-electronic-excitation subspace, the standard Hamiltonian for a strongly coupled pigment-protein complex [26, 28, 29] then reduces to

$$\begin{aligned}
 H = & \epsilon_1|1\rangle\langle 1| + \epsilon_2|2\rangle\langle 2| + \epsilon_3|3, 0\rangle\langle 3, 0| \\
 & + (\epsilon_3 + \omega)|3, 1\rangle\langle 3, 1| \\
 & + J_{12}(|1\rangle\langle 2| + |2\rangle\langle 1|) + J_{23}(|2\rangle\langle 3, 0| + |3, 0\rangle\langle 2|) \\
 & + J_{13}(|1\rangle\langle 3, 0| + |3, 0\rangle\langle 1|) \\
 & + \lambda(|3, 0\rangle\langle 3, 1| + |3, 1\rangle\langle 3, 0|),
 \end{aligned}
 \tag{1}$$

where ϵ_i is the electronic excitation energy of site i and J_{ij} is the excitonic coupling between levels i and j .

The remaining vibrational modes of the pigment-protein complex and its environment are taken as a thermal bath and treated within the Lindblad formalism [30]. Three major effects of the bath are taken into account, shown as dashed and dotted arrows in Fig. 1. Each of the sites undergoes pure dephasing with respect to $|g\rangle$ at the rate γ_{deph} , assumed to be equal for all three sites. The two vibrational states of site 3 are treated as a single subspace as regards electronic dephasing. Interaction of the bath with the vibrational mode causes the mode

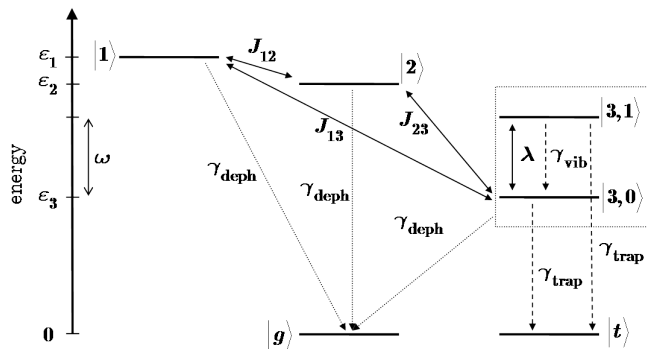


FIG. 1: Diagram of the three-site model, with site 3 coupled to a vibrational mode that is restricted to either 0 or 1 excitation(s). Solid arrows indicate coherent couplings, dashed arrows indicate irreversible decay pathways, and dotted arrows indicate dephasing pathways.

to decay from its excited state $|3,1\rangle$ to its ground state $|3,0\rangle$ with rate γ_{vib} . Finally, we add a trapping state $|t\rangle$ that absorbs energy from both vibronic levels on site 3 at rate γ_{trap} . For simplicity we neglect losses from exciton recombination or other non-radiative decay processes which occur on nanosecond timescales [6], much slower than the $\sim 0.5 - 5$ ps timescales we are interested in.

To ensure that our model is both physically motivated and realistic, parameter values used in the discussion of the model and numerical simulations are drawn from experimental results wherever possible. Exact values for the site energies and excitonic couplings vary depending on the organism being studied and the details of experimental spectra and theoretical fitting methods [6]. However, certain trends are clear. The relations $\epsilon_1 \sim \epsilon_2 > \epsilon_3$, $J_{12} > J_{23} > J_{13}$, $J_{12} \gg |\epsilon_1 - \epsilon_2|$ and $\epsilon_2 - \epsilon_3 \gg J_{23}$ are useful in obtaining physical insight into the model. For numerical calculations we use site energies and excitonic couplings from [26], as shown in Table I.

Site energies		Couplings	
ϵ_1	12475	J_{12}	-98.2
ϵ_2	12460	J_{13}	5.4
ϵ_3	12225	J_{23}	30.5

TABLE I: Parameter values in cm^{-1} for *Prosthecochloris aestuarii*, taken from [26].

The magnitude of the vibrational coupling constant λ requires careful consideration. This term originates from the shift of the nuclear normal-mode potential energy surface upon electronic excitation of a pigment molecule [28, 29], from which $\lambda = \omega\sqrt{S_\omega}$ where S_ω is the Huang-Rhys factor of the vibrational mode with frequency ω . Adolphs and Renger [26] considered a vibrational spectral density consisting of a broad continuous background with a single high-frequency mode at $\omega_H = 180 \text{ cm}^{-1}$. Comparing this model with the experimental vibrational spectra of Wendling *et al.* [13], they

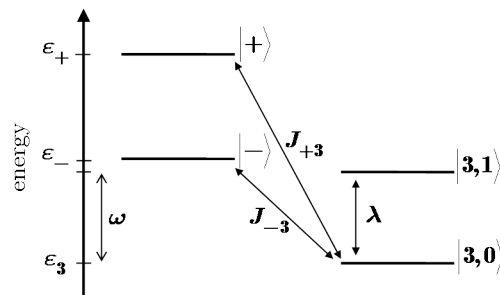


FIG. 2: Simplified model illustrating the resonance mechanism within a perturbative framework. The delocalised excitonic states $|\pm\rangle$ diagonalise the $\{|1\rangle, |2\rangle\}$ subspace. The transformed couplings $J_{\pm 3}$ are of similar magnitude to λ , which is much smaller than $\epsilon_{\pm} - \epsilon_3$. When $\omega \simeq \epsilon_{\pm} - \epsilon_3$, a resonance occurs and the exciton state $|\pm\rangle$ becomes strongly mixed with the vibrationally excited state $|3,1\rangle$ even though the states are only coupled to second order (via the intermediate state $|3,0\rangle$) and both $J_{\pm 3}$ and λ are small.

estimated the Huang-Rhys factor $S_H = 0.22$. Subsequent work has used the same or similar values [10, 11]. However, the Huang-Rhys factors for individual modes found in the experiments of Wendling *et al.* are on the order of $S_\omega \lesssim 0.01$, and in fact the sum of the Huang-Rhys factors for the thirty measured vibrational modes is on the order of $S_{\text{tot}} \sim 0.25$ [13]. As the physics presented here is based on a resonance mechanism and therefore relies on close frequency matching, we choose the Huang-Rhys factor $S_\omega \sim 0.01$ appropriate to an individual mode rather than the value $S \sim 0.2$ that corresponds to an effective coupling to a large number of modes. For the frequencies of interest in our model this yields $\lambda \sim 15 \text{ cm}^{-1}$, so that $\lambda < J_{23} < J_{12}$.

From the relations among the various energies and coupling strengths discussed above, we can extract a simplified picture that provides good intuition for the physics of the model. States $|1\rangle$ and $|2\rangle$ are near resonance and strongly coupled, so they must be treated in the delocalized ‘exciton basis’. This produces the set of basis states and couplings illustrated in Fig. 2: the new states $|\pm\rangle$ with energies ϵ_{\pm} are the excitonic states spanning the $\{|1\rangle, |2\rangle\}$ subspace, $J_{\pm 3}$ denotes their couplings to state $|3,0\rangle$, and the coupling λ between $|3,0\rangle$ and $|3,1\rangle$ remains unchanged. For our system $|J_{\pm 3}| \gtrsim \lambda$ and all three couplings are small enough to be treated as perturbative parameters. As long as ω is chosen so that $|3,1\rangle$ does not come into resonance with $|\pm\rangle$, the eigenstates will not vary significantly from the basis states. However, when $\omega \simeq \epsilon_{\pm} - \epsilon_3$ a resonance is created and $|3,1\rangle$ can become strongly mixed with $|\pm\rangle$.

The effect of the resonance may be analysed within this picture using degenerate perturbation theory. The Hamiltonian is divided into a ‘bare’ term H_0 and a per-

turbation term H' :

$$H = H_0 + H', \quad (2)$$

$$H_0 = \epsilon_+|+\rangle\langle+| + \epsilon_-|-\rangle\langle-| + \epsilon_3|3,0\rangle\langle 3,0| + (\epsilon_3 + \omega)|3,1\rangle\langle 3,1|, \quad (3)$$

$$H' = J_{+3}(|+\rangle\langle 3,0| + |3,0\rangle\langle+|) + J_{-3}(|-\rangle\langle 3,0| + |3,0\rangle\langle-|) + \lambda(|3,0\rangle\langle 3,1| + |3,1\rangle\langle 3,0|). \quad (4)$$

For notational simplicity we will take the resonant pair of states to be $|-\rangle$ and $|3,1\rangle$, so that $\omega = \epsilon_- - \epsilon_3$. The resulting degeneracy in H_0 creates divergences in the series expansions of the eigenstates of H . Therefore the first step in applying perturbation theory must be to identify the appropriate superpositions of the resonant states that will remove the degeneracy.

Looking at Eq. (2) it is immediately evident that there is no matrix element of H' that directly connects the two resonant states, so the degeneracy cannot be removed by simply diagonalising the degenerate subspace of H . It is necessary, then, to work to second order in the expansion of the eigenstates and energies [31] to determine an *effective* perturbation Hamiltonian \tilde{H} in the $\{|-\rangle, |3,1\rangle\}$ subspace. For two states $|m\rangle$ and $|l\rangle$ with $E_m = E_l$ the general form of \tilde{H} may be expressed as

$$\tilde{H} = \tilde{H}_{mm}|m\rangle\langle m| + \tilde{H}_{ll}|l\rangle\langle l| + (\tilde{H}_{ml}|m\rangle\langle l| + \text{H.c.}), \quad (5)$$

where H.c. denotes Hermitian conjugate and the matrix elements are given by

$$\tilde{H}_{mm} = \sum_{n \neq l, m} \frac{|\langle n|H'|m\rangle|^2}{E_m - E_n}, \quad (6)$$

$$\tilde{H}_{ll} = \sum_{n \neq l, m} \frac{|\langle n|H'|l\rangle|^2}{E_m - E_n}, \quad (7)$$

$$\tilde{H}_{ml} = \sum_{n \neq l, m} \frac{\langle m|H'|n\rangle\langle n|H'|l\rangle}{E_m - E_n}. \quad (8)$$

The sum is taken over the remaining nondegenerate states of the bare Hamiltonian. By diagonalising \tilde{H} and taking its eigenstates as the new basis states for the perturbation calculation, the degeneracy that would otherwise cause the expansions to diverge may be removed.

In the present case each of the degenerate states couples only to $|3,0\rangle$ so that the sums reduce to a single term each and we obtain

$$\tilde{H} = \frac{|J_{-3}|^2}{\omega}|-\rangle\langle-| + \frac{|\lambda|^2}{\omega}|3,1\rangle\langle 3,1| + \frac{J_{-3}\lambda}{\omega}(|-\rangle\langle 3,1| + |3,1\rangle\langle-|), \quad (9)$$

where $J_{-3} = \langle 3,0|H'|-\rangle = c_1^- J_{13} + c_2^- J_{23}$ is the coupling between the state $|-\rangle = c_1^-|1\rangle + c_2^-|2\rangle$ and the intermediate state $|3,0\rangle$.

Inspection of Eq. (9) shows that, in fact, $\omega = \epsilon_- - \epsilon_3$ is not the exact resonance frequency of the interacting

system unless $|J_{-3}|^2 = |\lambda|^2$. The interaction of $|-\rangle$ ($|3,1\rangle$) with $|3,0\rangle$ shifts its energy, and if the interaction strengths are different the states will be shifted slightly out of resonance. This effect may be accounted for by adding a further perturbation term

$$H'' = \delta\omega|3,1\rangle\langle 3,1| \quad (10)$$

that allows the resonance frequency ω to be adjusted. This term acts only to second order in the perturbation expansion, so it does not correct the degeneracy to first order. To second order the effective Hamiltonian becomes

$$\tilde{H} = \frac{|J_{-3}|^2}{\omega}|-\rangle\langle-| + \left(\frac{|\lambda|^2}{\omega} + \delta\omega\right)|3,1\rangle\langle 3,1| + \frac{J_{-3}\lambda}{\omega}(|-\rangle\langle 3,1| + |3,1\rangle\langle-|). \quad (11)$$

The condition for exact resonance is that the diagonal terms of \tilde{H} are equal, which occurs when

$$\delta\omega = \frac{|J_{-3}|^2 - |\lambda|^2}{\omega}. \quad (12)$$

At this point the energy corrections due to interactions within the degenerate subspace are $\tilde{E}_1 = -\tilde{E}_2 = J_{-3}\lambda/\omega$ and the original basis states $|-\rangle$ and $|3,1\rangle$ are maximally mixed. To get an idea of how well our degenerate perturbation theory analysis works for the FMO complex, we can compare it against a numerical solution of the full system. The resonance frequencies may be found by using the simulations to identify the avoided crossings of the eigenvalues of H as a function of ω , which gives $\omega \approx 147.1 \text{ cm}^{-1}$ for the lower resonance. Perturbation theory predicts a resonance frequency $\omega + \delta\omega = 147.1 \text{ cm}^{-1}$ in excellent agreement with the numerical result. Likewise the energy splitting $2J_{-3}\lambda/\omega = 5.4 \text{ cm}^{-1}$, which agrees well with the numerical values of 5.1 cm^{-1} .

The same analysis may be applied when ω is such that $|3,1\rangle$ is on resonance with the upper excitonic state $|+\rangle$. A prediction of $\omega + \delta\omega = 341.2 \text{ cm}^{-1}$ is obtained. However, in this case the couplings J_{13} and J_{23} add destructively, giving $J_{+3} = -16.8 \text{ cm}^{-1}$, somewhat smaller than $J_{-3} = 25.9 \text{ cm}^{-1}$. Together with the larger resonance frequency, this produces an energy splitting of just 0.7 cm^{-1} . Consequentially the effect of the resonance with $|+\rangle$ on the dynamics of the system is much smaller than that of $|-\rangle$. This is not inconsistent with the relaxation pathways proposed by Brixner *et al.* [27], in which exciton 7 (roughly equivalent to $|+\rangle$ in our model) decays to exciton 3 ($|-\rangle$ in our model) rather than directly to the lowest level primarily localised on site 3. Given the small energy difference and large coupling between sites 1 and 2, this transition seems unlikely to be vibrationally assisted in the coherent sense discussed here. Alternatively, Chin *et al.* [10] suggest that $|+\rangle$ may couple strongly to one of the exciton states on sites 4-7 of FMO, so it may participate in a more complicated energy transfer mechanism that is not captured in our simplified

model. Therefore we will focus on the resonance with $|-\rangle$ in the dynamical simulations to follow.

Despite its apparent simplicity, the model we have constructed captures the interplay between delocalised exciton states and local vibrational modes. It is worth emphasising that the coupling of the $|-\rangle$ and $|+\rangle$ excitonic states to the vibrationally excited state $|3,1\rangle$ is weak, as is the coupling between $|3,0\rangle$ and $|3,1\rangle$. Nevertheless, when the resonance condition is satisfied the exciton state becomes strongly mixed with the vibrationally excited state, creating delocalised vibronic states. The analytical framework provides both an intuitive picture for how resonance can contribute to energy transport and a solid mathematical method for accurately calculating resonance frequencies and the consequent splitting of the vibronic eigenstates. Within this model we can now study how vibronic resonances together with electronic coupling and environmental noise can contribute to energy transfer processes.

III. DYNAMICS OF ENERGY TRANSFER

In keeping with the spirit of simplicity, the dynamics of the system including the dephasing and decay pathways shown in Fig. 1 are calculated from a Markovian master equation [30], given by ($\hbar = 1$)

$$\frac{d\rho}{dt} = -i[H, \rho(t)] - \mathcal{L}_{\text{vib}}(\rho(t)) - \mathcal{L}_{\text{deph}}(\rho(t)) - \mathcal{L}_{\text{trap}}(\rho(t)) \quad (13)$$

where $\rho(t)$ is the density matrix of the system consisting of the three sites plus the vibrationally excited state. Decay of the vibrational excitation is described by the Lindblad superoperator

$$\mathcal{L}_{\text{vib}}(\rho(t)) = \gamma_{\text{vib}} \left(\frac{1}{2} \{ |3,1\rangle\langle 3,1|, \rho \} - |3,0\rangle\langle 3,1| \rho |3,1\rangle\langle 3,0| \right), \quad (14)$$

where $\{A, B\}$ denotes the anticommutator. The decay rate is taken as $\gamma_{\text{vib}} = 7.5 \text{ cm}^{-1} = 0.23 \text{ ps}^{-1}$ based on the experimental results of Wendling *et al.* [13]. The dephasing operator is given by

$$\mathcal{L}_{\text{deph}}(\rho(t)) = \gamma_{\text{deph}} \sum_{i=1,2} \left(\frac{1}{2} \{ L_i^\dagger L_i, \rho \} - L_i \rho L_i^\dagger \right). \quad (15)$$

The dephasing on sites 1 and 2 follows the usual definition, so $L_i = |g\rangle\langle g| - |i\rangle\langle i|$ for $i = 1, 2$. For site 3 the form of the dephasing operator has been chosen such that the two vibrational levels $|3,0\rangle$ and $|3,1\rangle$ undergo the same dephasing process: $L_3 = |g\rangle\langle g| - \frac{1}{2}(|3,0\rangle\langle 3,0| + |3,1\rangle\langle 3,1|)$. The dephasing rate γ_{deph} is assumed to be the same for all sites. Transfer of excitation energy to the reaction center is modelled by an irreversible decay to the trapping site $|t\rangle$ with rate γ_{trap} and Lindblad operator

$$\mathcal{L}_{\text{trap}}(\rho(t)) = \gamma_{\text{trap}} \left(\frac{1}{2} \{ |3,0\rangle\langle 3,0|, \rho \} + \frac{1}{2} \{ |3,1\rangle\langle 3,1|, \rho \} - |t\rangle\langle 3,0| \rho |3,0\rangle\langle t| - |t\rangle\langle 3,1| \rho |3,1\rangle\langle t| \right). \quad (16)$$

Without dephasing or trapping it should be immediately clear that adding a resonant vibrational level provides a dramatic improvement in energy transport across the system. In the absence of the vibrational mode, the large energy gap and small coupling between site 3 and the rest of the system means that initial excitation of site 1 produces an oscillatory population on site 3 with a maximum amplitude of about 2.5%. In our model the effective Hamiltonian given in Eq. (11) suggests that an excitation in $|-\rangle$ will be completely transferred to state $|3,1\rangle$ at time $\tau = (\pi/2)(\hbar\omega/J\lambda) \approx 3 \text{ ps}$, which is of the right order to be of biological relevance. Adding decay to the vibrational mode provides directionality of energy transport. On resonance and with $\gamma_{\text{vib}} = 7.5 \text{ cm}^{-1}$, the population of $|3,0\rangle$ reaches 40% after 5 ps following an initial excitation on site 1. The final population is primarily limited by the amplitude of $|-\rangle$ in the initial state, as $|+\rangle$ couples very weakly to $|3,0\rangle$.

Biological systems, however, operate under conditions in which dephasing cannot be neglected; indeed, dephasing has been shown to enhance energy transport in a variety of biologically relevant models [7, 8, 10, 11]. In order to evaluate the effect of vibrational resonance, Eq. (13) was used to calculate the population P_{trap} of the trap site $|t\rangle$ at time $t = 5 \text{ ps}$, following an initial excitation in state $|1\rangle$. The value of $\gamma_{\text{trap}} = 1 \text{ cm}^{-1} = 0.03 \text{ ps}^{-1}$ was chosen to be similar to that of Refs. [7, 8]. Figure 3 shows the results as a function of the vibrational frequency ω and the dephasing rate γ_{deph} . At small dephasing, a significant enhancement of the trap population is found for $\omega \sim 147 \text{ cm}^{-1}$, corresponding to the resonance between $|-\rangle$ and $|3,1\rangle$. A smaller peak due to the resonance with $|+\rangle$ is visible around $\omega = 341 \text{ cm}^{-1}$. As the dephasing increases the effect of the resonance diminishes but remains visible up to the highest values considered. In our equations the parameter γ_{deph} produces an exponential decay of coherences at rate $2\gamma_{\text{deph}}$, so $\gamma_{\text{deph}} = 75 \text{ cm}^{-1}$ maps onto the room temperature decoherence rate of the exciton 1-3 coherence oscillations measured experimentally [32]. Although the value of γ_{deph} appropriate to our model cannot be extracted from such experiments, the results do tend to suggest that some improvement due to vibrational-assisted resonance could persist even up to biologically relevant temperatures.

Irreversible decay to a trapping site is a typical feature of dephasing-assisted transport models [7, 8, 10, 11]. Indeed, when the effect of environmental noise is limited to pure dephasing described within the Lindblad formalism, the trapping process is critical to ensuring effective transport. Otherwise the system evolves smoothly to a steady-state population determined by the temperature; in zero-temperature models, as here, the final population on each site is $1/N$ where N is the number of sites in the network [8]. Inclusion of the trapping process is justified by the belief that the FMO protein functions as a ‘molecular wire’ that transmits energy from the chlorosome antenna complex to the reaction center [5]. Unfortunately there is very little data about the kinetics of

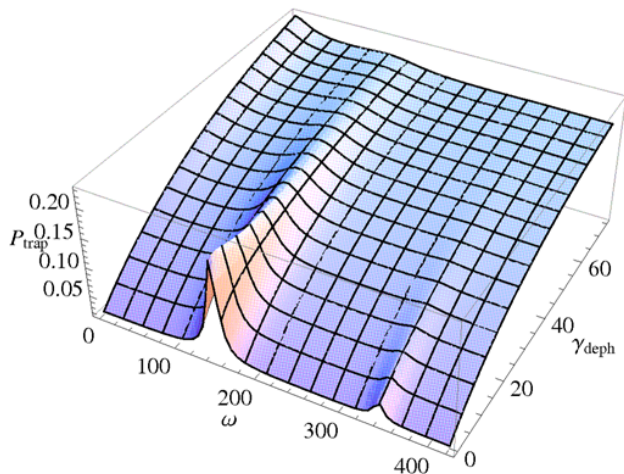


FIG. 3: Trap state population P_{trap} at 5 ps for an initial state on site 1 as a function of vibrational frequency ω and dephasing rate γ_{deph} (both measured in cm^{-1}). The trapping rate has been set to $\gamma_{\text{trap}} = 1 \text{ cm}^{-1}$. Peaks at $\omega \approx 147 \text{ cm}^{-1}$ and 341 cm^{-1} correspond to resonances of $|-\rangle$ and $|+\rangle$ with $|3, 1\rangle$.

energy transfer from FMO to the reaction center; what few experiments exist have shown surprisingly slow and inefficient transfer, in contradiction to expectations from structural evidence [12]. Experiments on other antenna-reaction center complexes have shown that traps spend some fraction of time closed to further energy transfer and also that excitons may have a nontrivial probability of escaping from the trap back into the antenna [4, 12]. In FMO neither the trapping rate nor the nature of the trapping process is known, indicating that caution should be used in drawing conclusions from models that rely heavily on a trapping mechanism that may or may not be physically realistic.

With that caveat in mind, it is interesting to look at how the vibration-assisted resonance model behaves in the absence of trapping. Figure 4 shows the population of $|3, 0\rangle$ in the absence of trapping both with (a) and without (b) vibrational coupling. Without the vibrational coupling, setting $\gamma_{\text{deph}} = 0$ demonstrates the very poor energy transport properties of purely coherent dynamics. Finite dephasing values all lead to a steady-state population of $1/3$; the larger the dephasing, the faster this state is achieved. In the vibrational case with $\gamma_{\text{deph}} = 0$, the steady-state population is determined by the amplitude of $|-\rangle$ in the initial state $|1\rangle$, here nearly one-half. Adding a small amount of dephasing allows the initial population in $|+\rangle$ to be transferred with high probability. However, increasing the dephasing beyond a certain optimal value (here around 2 cm^{-1}) reduces the population transfer. At sufficiently large dephasing values the diffusion limit is recovered, in which the population of $|3, 0\rangle$ rises quickly to its steady-state value. The vibration-assisted increase in transfer efficiency appears

to be quite sensitive to the precise dephasing rate and reaches its peak value over a relatively long timescale. On the other hand, the improvement is caused by the inclusion of the decay term on the vibrational mode, a process that has a sound physical basis. It is interesting to note that varying γ_{vib} (not shown) indicates that, on resonance, the energy transfer is optimised at a value very close to the linewidth of 7.5 cm^{-1} obtained in vibrational spectroscopy experiments [13].

A further feature of resonance is that it substantially reduces the sensitivity of the trap population to the trapping rate γ_{trap} , as illustrated in Fig. 5. The difference is especially pronounced in the relatively small trapping regime which seems more likely to be relevant in FMO. Such an insensitivity might be advantageous if the trapping rate varies depending on whether an excitation has already been transferred to the reaction center.

IV. DISCUSSION

Our numerical simulations show that vibration-assisted resonance can increase energy transport efficiency within a simple mathematical model, although the results should apply quite generally in more complicated networks. Where possible, we have used parameters based on experimental data in order to get a sense of whether the mechanism could play a role in biological function. Of course it is not possible to directly compare our minimal model with experimental results; nevertheless, a few remarks are in order.

Comparison of the resonant frequencies obtained in our three-site model with the vibrational frequencies obtained in the experiments of Wendling *et al.* [13] shows that our calculated frequencies actually fall in gaps in the vibrational spectrum. To a certain extent this is because we consider only three sites of the FMO complex; coupling to the remaining sites provides further shifts to the exciton levels $|\pm\rangle$, which will alter the values of ω . More fundamentally, the resonance frequency depends strongly on the particular values chosen for the site energies and exciton couplings. As yet there is no direct experimental method for measuring the site energies, and values based on theoretical fits to experimental spectra vary considerably [6]. In order to estimate the sensitivity of the frequency to changes in the Hamiltonian, we calculated resonance frequencies from a number of published data sets for the site energies and exciton couplings in the FMO complex of *P. aestuarii*. Values for the lower resonance ranged from 94 to 167 cm^{-1} . From this exercise we conclude that the site energies, in particular, of FMO are not yet sufficiently well known to enable accurate calculation of resonance frequencies.

Recent experiments have been designed to address the hypothesis that vibrational and/or vibronic coherence might be responsible for the observed quantum beating in FMO. Hayes *et al.* studied FMO complexes with modified vibronic structure and found little effect on the fre-

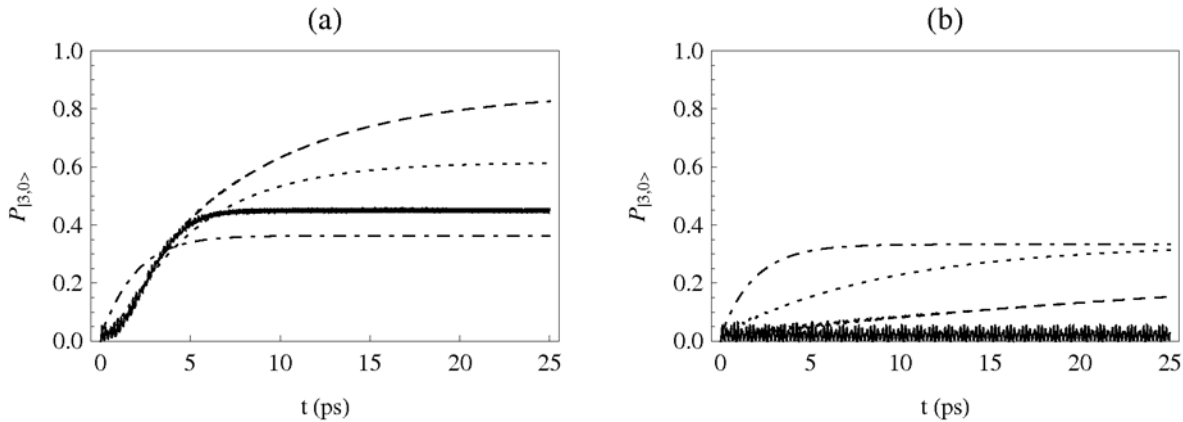


FIG. 4: Population of $|3,0\rangle$ ($P_{|3,0\rangle}$) in the absence of trapping for an initial excitation on site 1, both with (a) and without (b) vibrational coupling. Dephasing values (in cm^{-1}) are $\gamma_{\text{deph}} = 0$ (solid), 2 (dashed), 10 (dotted), and 50 (dot-dashed). A longer timescale of 25 ps has been chosen to show the steady-state behaviour of the population.

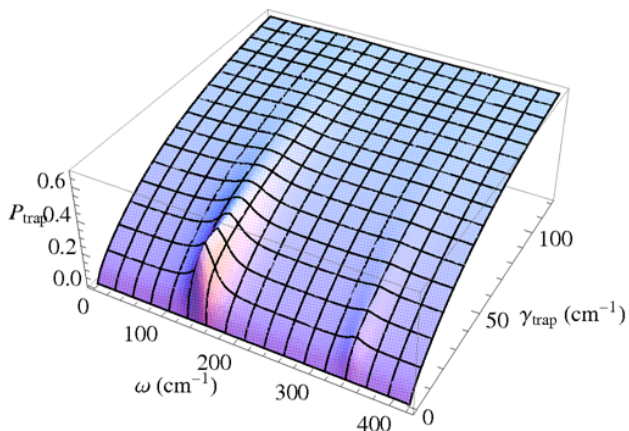


FIG. 5: Trap state population P_{trap} at 5 ps for an initial state on site 1 as a function of vibrational frequency ω and trapping rate γ_{trap} (both measured in cm^{-1}). The dephasing rate has been set to the small value $\gamma_{\text{deph}} = 2 \text{ cm}^{-1}$ so as not to obscure the dependence on the trapping rate. Peaks at $\omega \approx 147 \text{ cm}^{-1}$ and 341 cm^{-1} correspond to resonances of $|-\rangle$ and $|+\rangle$ with $|3,1\rangle$.

quency or dephasing of the beating in the exciton 1-2 crosspeak [33]. The beat frequency is equal to the energy difference between the two exciton levels. In our model, resonance with the vibrational mode has little effect on the energy difference since the splitting due to the resonance is small, about 5 cm^{-1} . Therefore we would not expect to observe much change in the coherence beat frequency when the vibrational mode is shifted off resonance. The primary effect of the resonance is an enhancement of the energy transfer efficiency, which was not addressed in that particular experiment. Another experiment designed to compare the 2D spectra of Bchl *a* in solution with the spectra of FMO was unable to resolve more than two vibrational modes, which had frequencies

well above those relevant for our model [34]. Neither of these experiments would seem to rule out a vibration-assisted resonance mechanism.

On the other hand, an experiment examining the inhomogeneous broadening of the exciton 1-3 coherence in FMO found the energy gap between the exciton levels to be quite consistent across the sample [35]. This is not necessarily a general feature of photosynthetic pigment-protein complexes, as the authors also studied the LH2 antenna complex from purple bacteria and found a large degree of inhomogeneous broadening. Their result supports the idea that having a well-defined exciton splitting is important to the functioning of the FMO complex. Such an interpretation would be more consistent with our model, which requires a close match between the exciton splitting and a specific vibrational frequency, than with the dephasing-assisted mechanism that places no restrictions on the exciton splittings. Ultimately, though, determining whether vibration-assisted resonance plays a significant role in biological function will require a better understanding of the kinetics and decoherence properties of pigment-protein complexes.

V. CONCLUSIONS

The vibration-assisted resonance mechanism presented here complements the now well accepted dephasing-assisted transport mechanism. In addition to increasing the speed and, in some cases, the overall probability of energy transfer, it reduces the dependence on a possibly unphysical trapping mechanism. While in this paper we have taken the dephasing rate to be equal for all sites, it will be interesting to look at how the optimisation of individual site dephasing rates changes with the inclusion of vibrational resonance. Within dephasing-assisted models, bridging large energy gaps requires corresponding large dephasing values. Since it permits efficient reso-

nant transport across these large gaps, vibration-assisted resonance may be expected to reduce the variation in dephasing rates required for optimal transfer.

Our work demonstrates that vibronic coherence is not necessarily irrelevant to energy transport, contradicting the conclusions of Christensson *et al.* [20]. The vibronic theory of Refs. [20, 25] neglects noise effects on the vibrational mode and focuses on vibrational coherences that are localised on a single pigment. In contrast, the results presented here show that the resonance-induced delocalisation of the mixed vibronic-excitonic states and the decay of vibrational excitations are key to the enhancement of transport. Indeed, by strongly mixing a vibrationally excited level on one site with the vibrational ground state of another site, our model creates an even greater degree of coherent delocalisation across the network than excitonic coupling alone.

Furthermore, our theory provides one possible framework for treating a small number of resonant vibrational levels explicitly within the system Hamiltonian. More generally, this is a possible way to model non-Markovian bath effects [36], and formal relationships between the spectral densities of the bath, for a system that in-

cludes or excludes a single bath coordinate can be derived [37, 38].

The conceptual and analytical framework developed here provides ample scope for further development. Comparisons with existing experiments will require extending the model to the full FMO complex and including multiple vibrational modes, together with the effects of finite temperature. This should enable better identification of appropriate vibrational modes and of which excitonic transitions might be vibrationally assisted. Beyond FMO, it will be interesting to look at other photosynthetic complexes in order to understand whether vibration-assisted resonance can be considered as a general principle of biological energy transport.

VI. ACKNOWLEDGEMENTS

This work was funded by the Leverhulme Trust. BWL thanks the Royal Society for a University Research Fellowship.

-
- [1] G. S. Engel, T. R. Calhoun, E. L. Read, T.-K. Ahn, T. Mančal, Y.-C. Cheng, R. E. Blankenship, and G. R. Fleming, *Nature* **446**, 782 (2007).
 - [2] G. Panitchayangkoon, D. V. Voronine, D. Abramavicius, J. R. Caram, N. H. C. Lewis, S. Mukamel, and G. S. Engel, *P. Natl. Acad. Sci. USA* **108**, 20908 (2011).
 - [3] R. J. Sension, *Nature* **446**, 740 (2007).
 - [4] R. E. Blankenship, *Molecular Mechanisms of Photosynthesis* (Blackwell Publishing, Oxford, 2002).
 - [5] J. M. Olson, *Photosynth. Res.* **80**, 181 (2004).
 - [6] M. T. W. Milder, B. Brüggemann, R. van Grondelle, and J. L. Herek, *Photosynth. Res.* **104**, 257 (2010).
 - [7] M. B. Plenio and S. F. Huelga, *New J. Phys.* **10**, 113019 (2008).
 - [8] P. Rebentrost, M. Mohseni, I. Kassal, S. Lloyd, and A. Aspuru-Guzik, *New J. Phys.* **11**, 033003 (2009).
 - [9] F. Caruso, A. W. Chin, A. Datta, S. F. Huelga, and M. B. Plenio, *J. Chem. Phys.* **131**, 105106 (2009).
 - [10] A. W. Chin, A. Datta, F. Caruso, S. F. Huelga, and M. B. Plenio, *New J. Phys.* **12**, 065002 (2010).
 - [11] A. W. Chin, S. F. Huelga, and M. B. Plenio, *Phil. Trans. R. Soc. A* **370**, 3638 (2012).
 - [12] J. Ames� and S. Neerken, *Photosynth. Res.* **73**, 73 (2002).
 - [13] M. Wendling, T. Pullerits, M. A. Przyjalowski, S. I. E. Vulto, T. J. Aartsma, R. van Grondelle, and H. van Amerongen, *J. Phys. Chem. B* **104**, 5825 (2000).
 - [14] M. Rätsep and A. Freiberg, *J. Lumin.* **127**, 251 (2007).
 - [15] A. B. Doust, C. N. J. Marai, S. J. Harrop, K. E. Wilk, P. M. G. Curmi, and G. D. Scholes, *J. Mol. Biol.* **344**, 135 (2004).
 - [16] V. I. Novoderezhkin, A. B. Doust, C. Curutchet, G. D. Scholes, and R. van Grondelle, *Biophys. J.* **99**, 344 (2010).
 - [17] G. Ritschel, J. Roden, W. T. Strunz, and A. Eisfeld, *New J. Phys.* **13**, 113034 (2011).
 - [18] M. del Rey, A. W. Chin, S. F. Huelga, and M. B. Plenio, *J. Phys. Chem. Lett.* **4**, 903 (2013).
 - [19] A. W. Chin, J. Prior, R. Rosenbach, F. Caycedo-Soler, S. F. Huelga, and M. B. Plenio, *Nat. Phys.* **9**, 113 (2013).
 - [20] N. Christensson, H. F. Kauffmann, T. Pullerits, and T. Mančal, *J. Phys. Chem. B* **116**, 7449 (2012).
 - [21] J. Lim, M. Tame, K. H. Yee, J.-S. Lee, and J. Lee, arXiv:1304.3967 (2013).
 - [22] C. Olbrich, T. L. C. Jansen, J. Liebers, M. Aghtar, J. Strümpfer, K. Schulten, J. Knoester, and U. Kleinekathöfer, *J. Phys. Chem. B* **115**, 8609 (2011).
 - [23] J. R. Caram, N. H. C. Lewis, A. F. Fidler, and G. S. Engel, *J. Chem. Phys.* **136**, 104505 (2012).
 - [24] A. Kolli, E. J. O'Reilly, G. D. Scholes, and A. Olaya-Castro, *J. Chem. Phys.* **137**, 174109 (2012).
 - [25] A. Chenu, N. Christensson, H. F. Kauffmann, and T. Mančal, arXiv:1211.4397 (2012).
 - [26] J. Adolphs and T. Renger, *Biophys. J.* **91**, 2778 (2006).
 - [27] T. Brixner, J. Stenger, H. M. Vaswani, M. Cho, R. E. Blankenship, and G. R. Fleming, *Nature* **434**, 625 (2005).
 - [28] J. M. Jean, R. A. Friesner, and G. R. Fleming, *J. Chem. Phys.* **96**, 5827 (1992).
 - [29] T. Renger, V. May, and O. Kühn, *Phys. Rep.* **343**, 137 (2001).
 - [30] H.-P. Breuer and F. Petruccione, *The Theory of Open Quantum Systems* (Oxford University Press, Oxford, 2002).
 - [31] L. I. Schiff, *Quantum Mechanics* (McGraw-Hill, New York, 1968), 3rd ed.
 - [32] G. Panitchayangkoon, D. Hayes, K. A. Fransted, J. R. Caram, E. Harel, J. Wen, R. E. Blankenship, and G. S. Engel, *P. Natl. Acad. Sci. USA* **107**, 12766 (2010).

- [33] D. Hayes and G. S. Engel, *Biophys. J.* **100**, 2043 (2011).
- [34] K. A. Fransted, J. R. Caram, D. Hayes, and G. S. Engel, *J. Chem. Phys.* **137**, 125101 (2012).
- [35] A. F. Fidler, E. Harel, P. D. Long, and G. S. Engel, *J. Phys. Chem. A* **116**, 282 (2012).
- [36] J. C. Iles-Smith et al., unpublished (2013).
- [37] M. P. Woods, R. Groux, A. W. Chin, S. F. Huelga, and M. B. Plenio, arXiv:1111.5262 (2011).
- [38] A. Garg, J. N. Onuchic, and V. Ambegaokar, *J. Chem. Phys.* **83**, 4491 (1985).